

Assessing Radar Waveforms for Spectral Coexistence via the PARSAX System

Aubry, A.; Carotenuto, V.; Maio, A. De; Fioranelli, F.; Krasnov, O.; Yarovoy, A.; Zwan, F. van der

וסמ

10.1109/TAES.2024.3412867

Publication date

Document VersionFinal published version

Published in

IEEE Transactions on Aerospace and Electronic Systems

Citation (APA)

Aubry, A., Carotenuto, V., Maio, A. D., Fioranelli, F., Krasnov, O., Yarovoy, A., & Zwan, F. V. D. (2024). Assessing Radar Waveforms for Spectral Coexistence via the PARSAX System. *IEEE Transactions on Aerospace and Electronic Systems*, *60*(5), 6671-6684. https://doi.org/10.1109/TAES.2024.3412867

Important note

To cite this publication, please use the final published version (if applicable). Please check the document version above.

Copyright

Other than for strictly personal use, it is not permitted to download, forward or distribute the text or part of it, without the consent of the author(s) and/or copyright holder(s), unless the work is under an open content license such as Creative Commons.

Takedown policy

Please contact us and provide details if you believe this document breaches copyrights. We will remove access to the work immediately and investigate your claim.

Green Open Access added to TU Delft Institutional Repository 'You share, we take care!' - Taverne project

https://www.openaccess.nl/en/you-share-we-take-care

Otherwise as indicated in the copyright section: the publisher is the copyright holder of this work and the author uses the Dutch legislation to make this work public.

Assessing Radar Waveforms for Spectral Coexistence via the PARSAX System

AUGUSTO AUBRY , Senior Member, IEEE
VINCENZO CAROTENUTO , Senior Member, IEEE
ANTONIO DE MAIO , Fellow, IEEE
University of Naples Federico II, Naples, Italy

FRANCESCO FIORANELLI , Senior Member, IEEE OLEG KRASNOV
ALEXANDER YAROVOY, Fellow, IEEE FRED VAN DER ZWAN
Delft University of Technology, Delft, The Netherlands

This article focuses on the experimental validation of probing signals designed to enable radar operation in spectrally crowded environments using an S-band software defined radar (SDR). The tested waveforms ensure spectral coexistence between the sensing system and frequency-overlaid emitters, while optimizing radar performance. This is achieved through a bespoke notching of the radar signal spectrum to control the amount of interference injected by the radar in each shared frequency interval. In addition, some relevant

system and frequency-overlaid emitters, while optimizing radar performance. This is achieved through a bespoke notching of the radar signal spectrum to control the amount of interference injected by the radar in each shared frequency interval. In addition, some relevant features of the probing signal that influence radar performance are controlled via a similarity index, describing the maximum allowable distance between the spectrally notched waveform and a prescribed radar signal. In a first stage, the study is aimed at verifying whether the transmit and receive chains of the SDR system impair the spectral and temporal features of the designed waveforms. Subsequently, the

Manuscript received 8 February 2024; accepted 23 May 2024. Date of publication 11 June 2024; date of current version 11 October 2024.

DOI. No. 10.1109/TAES.2024.3412867

Refereeing of this contribution was handled by Justin Metcalf.

The work of A. Aubry and A. De Maio was supported in part by the European Union under the Italian National Recovery and Resilience Plan (NRRP) of NextGenerationEU, partnership on "Telecommunications of the Future" (PE00000001 - program "RESTART"). The work of V. Carotenuto was supported by the Research Program PON R&I under Grant AIM1878982-1.

Authors' addresses: Augusto Aubry, Vincenzo Carotenuto, and Antonio De Maio are with the University of Naples Federico II, 80125 Naples, Italy, E-mail: (augusto.aubry@unina.it; vincenzo.carotenuto@unina.it; ademaio@unina.it); Francesco Fioranelli, Oleg Krasnov, Alexander Yarovoy, and Fred van der Zwan are with the Department of Microelectronics, 2628CD Delft, The Netherlands, E-mail: (f.fioranelli@tudelft.nl; O.A. Krasnov@tudelft.nl; a.yarovoy@tudelft.nl; w.f.vanderzwan@tudelft.nl). (Corresponding author: Vincenzo Carotenuto.)

tested signals are radiated into the environment to investigate their effectiveness to detect targets in the illuminated scene, as well as to ensure spectral coexistence in the presence of frequency-overlaid emitters. The results demonstrated that by exploiting the designed radar probing signals, the SDR system is capable of sharing spectrum with other radio frequency wireless systems while also allowing to detect both stationary and moving targets.

I. INTRODUCTION

The ever-growing demands for spectral resources in wireless communication services have resulted in a crowding phenomenon of the radio frequency (RF) spectrum, especially in frequency bands traditionally employed by radar systems [1], [2], [3]. This problem has prompted the development of spectrum-sharing strategies aimed at enabling the cohabitation of radar and other RF emitters within the same spectral interval [4], [5], [6], [7].

To effectively capitalize on available spectral resources without interfering with other frequency-overlaid systems, the cognitive radar paradigm is recognized within the radar community as a highly promising solution [8], [9], [10], [11], [12], [13]. It leverages the use of a sensing module to gain awareness of the actual spectrum allocation and exploits the gathered information to synthesize radar probing waveforms tailored to the observed interference environment [14], [15], [16], [17], [18], [19], [20], [21], [22], [23], [24], [25], [26], [27], [28], [29], [30], [31].

Despite many strategies relying on the cognitive radar paradigm (whether oriented toward spectrum sensing, radar waveform synthesis, or both) have shown promising results during their validation on simulated data, it is crucial to conduct additional tests using experimental testbeds to confirm their effectiveness in practical scenarios. This type of study is essential for the practical successful application of the techniques [32], [33], [34], [35], [36], [37], [38], [39], [40], [41], [42], [43], [44], [45], [46], [47].

With respect to probing waveform synthesis, among the techniques available in open literature, the algorithm proposed in [19] enables a radar to coexist with frequencyoverlaid wireless systems, while optimizing the signal-tointerference plus noise ratio (SINR). This is achieved by placing bespoke notches in the probing signal spectrum, allowing control over the amount of interference injected by the radar in each shared frequency interval (hereafter referred to as stop bands). The design parameters are the individual width and depth of each notch, as well as a similarity-like index describing the maximum allowable distance from a prescribed radar waveform. It permits to control some relevant features of the radar probing signal, such as variations in the signal modulus as well as integrated sidelobe level (ISL) and peak-to-sidelobe level (PSL). The technical feasibility of this strategy has been studied in [46] and [47] through experimental validations using hardware-in-the-loop testbeds, also accounting for possible distortions induced on the synthesized spectrally notched signal by power amplifiers (PAs). However, to achieve a higher technology readiness level (TRL) validation of the framework, it is necessary to radiate the designed

^{© 2024} The Authors. This work is licensed under a Creative Commons Attribution 4.0 License. For more information, see https://creativecommons.org/licenses/by/4.0/

waveform into the environment and assess both spectral coexistence and radar performance.

Given the outlined context, this article aims to investigate the effectiveness of spectrally notched waveforms when used as input in a software-defined radar (SDR). The study is conducted through a measurement campaign involving the use of the PARSAX system, a fully polarimetric S-band SDR located on the roof of the Electrical Engineering, Mathematics & Computer Science (EEMCS) facility at TU Delft in The Netherlands. The radar offers the capability to use customized digital waveforms generated via an arbitrary waveform generator (AWG) as probing signals. In addition, it provides a calibration mode beyond the conventional sensing mode, which can be used for testing the characteristics of the radar waveform before being radiated into the environment.

Leveraging the aforementioned capabilities, in this study, the PARSAX system is operated as a pulsed radar by feeding its AWG with waveforms designed via the considered algorithm [19]. Furthermore, both the sensing and calibration modes are employed to investigate the effects of the radar transmit and receive chain on the synthesized spectrally notched signals. The initial assessment focuses on establishing whether the signals generated by the SDR system conform to their theoretical counterparts. Subsequently, the synthesized waveforms are radiated into the environment across various scenarios to study their capability to detect both stationary and moving targets. Finally, spectral coexistence between the radiated spectrally notched probing signals and frequency-overlaid communication signals is studied, by verifying whether the interference produced by the sensing system in the shared frequency bands compromises the communication links.

The results show that the spectrally notched signals once radiated into the environment, still comply with the requirements specified at the design stage, ensuring spectral coexistence with frequency-overlaid RF emitters. Moreover, processing the echoes backscattered from the environment and gathered at the radar receive side, the system is able to detect both stationary and moving targets.

The rest of this article is organized as follows. In Section II, a glimpse on the algorithm used for synthesizing spectrally notched radar waveforms is provided. In Section III, the main features of the PARSAX system are described. In Section IV, the results of the experimental analysis are discussed. Finally, Section V concludes this article.

II. WAVEFORM DESIGN

The waveform used for the experimental analysis is designed according to the algorithm proposed in [19]. It allows to: 1) enable coexistence between radar and wireless systems, 2) optimize radar detection performance, and 3) control some relevant hallmarks of the designed probing signal, such as range-Doppler resolution, signal modulus variations, (ISL, and PSL. Requirement 1 is satisfied by

limiting the interference level injected by the radar into the shared frequency intervals, condition 2 by maximizing the SINR, and requisite 3 by imposing similarity-like constraints on the designed radar code. More in detail, assuming awareness of the RF electromagnetic scenario surrounding the radar (gathered via a radio environment map or spectrum sensing [14], [15], [16], [17], [18]), the waveform design problem in [19] is formulated as

$$\mathcal{P} \begin{cases}
\text{maximize} & \text{SINR} \\
subject to} & I_k \leq \bar{I}_k, \ k = 1, \dots, K \\
 & \|\boldsymbol{c} - \alpha \boldsymbol{c}_0\|^2 \leq \epsilon \\
 & \|\boldsymbol{c}\|^2 \leq 1 \\
 & |\alpha|^2 \leq 1
\end{cases} \tag{1}$$

where $c \in \mathbb{C}^N$ and $c_0 \in \mathbb{C}^N$ ($\|c\|^2 = 1$), respectively, represent the radar sought and reference codes, $\epsilon \in [0, 1]$ rules the similarity level between c and c_0 , $\alpha \in \mathbb{C}$ enables the modulation of the energy of c_0 , K denotes the number of shared frequency bandwidths (referred to as stop-bands in the following), I_k and \bar{I}_k , k = 1, ..., K, indicate the actual and the maximum tolerable interference level in the kth stop-band, respectively. According to [19], problem \mathcal{P} can be equivalently recast as a nonconvex quadratically constrained quadratic program and approximatively solved leveraging a procedure based on semidefinite relaxation and randomization. The parameters to be specified at the design stage are the stop-bands where spectral coexistence is required along with the corresponding tolerable interference levels (i.e., the individual width and depth of each notch), the reference code, and the similarity parameter.

Unlike waveform design strategies where the spectral coexistence is achieved by primarily modulating the phase of the probing signal, the considered approach also capitalizes the degrees of freedom for the transmitted energy modulation.

Over the past years, the practical implementation of the aforementioned technique has already been investigated in [46] and [47] using hardware-in-the-loop testbeds and also accounting for possible distortions induced on the probing signal by the power amplification stage. In particular, in the presence of PAs operating within their linear region, the experimental analyses in [46] demonstrated the feasibility of generating spectrally notched radar waveforms complying with the desired spectral requirements. On the other hand, in the presence of PAs operating in nonlinear regime, the assessment in [47] highlighted a significant degradation in the spectral characteristics of the amplified signal, resulting in spectral compatibility impairments. Nonetheless, including a suitable predistortion stage upstream the PA provides a viable means to mitigate the PA distortions and achieve spectral coexistence.

Motivated by the results of previous investigations, this study completes the analysis focusing on a high TRL study case, involving the transmission of the synthesized spectrally notched radar waveform with an SDR, and assessing both radar performance and spectral coexistence.

¹Preliminary results on this study are shown in [48].



Fig. 1. PARSAX radar, located on the roof of the EEMCS facility at TU Delft, The Netherlands.

III. PARSAX SYSTEM

The PARSAX system [49], shown in Fig. 1 and located on the roof of the EEMCS facility at TU Delft in Delft, The Netherlands, is a highly reconfigurable, medium-range S-band fully polarimetric SDR equipped with two distinct antennas for simultaneous transmission and reception. It has high sensitivity, with transmit power up to +50 dBm per channel and receiver noise floor around -93 dBm; this allows to detect targets up to distances of a few tenths of kilometers, depending on their radar cross section (RCS). To prevent the saturation of the receiver circuits by the too strong reflected signal from the nearest objects, the transmit power can be set in two modes: 1) low power mode (+23 dBm) and 2) high power mode (+50 dBm).² In both cases, there is the possibility to control the transmit power using a digitally controlled attenuator with a 0.25-dB step within the range 0-64 dB. This extra attenuation can be selected from the radar control interface by the operator, or can be dynamically controlled burst by burst via an algorithm for automated transmit power control that prevents saturation of the radar receivers. Another relevant feature of the PARSAX is the availability of a calibration mode for testing the characteristics of the probing signals before being radiated into the environment.

Fig. 2 shows a high level schematic of the PARSAX system for a single polarimetric channel. As mentioned earlier, the PARSAX radar is designed as an SDR with digital signal processing implementation up to the intermediate frequency of 125 MHz. It includes a fully reprogrammable four-channel AWG that can generate signals based on the sequence of prerecorded waveform samples. These real-valued samples are representative of the probing waveform at the intermediate frequency of 125 MHz with the maximum bandwidth of ± 50 MHz. A copy of the signal at the output of the AWG is also gathered via a feedback/reference channel to perform customized signal processing.

The generated waveform is converted to RF at the S-band carrier of 3.315 GHz and amplified using either the

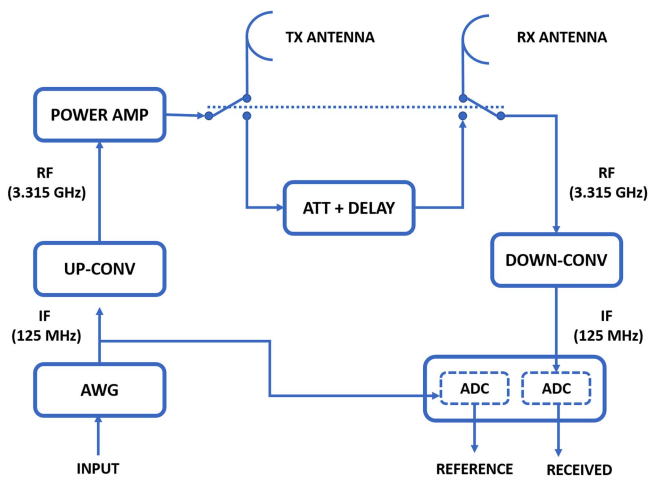


Fig. 2. Operating and calibration modes of the PARSAX system for a single polarimetric chanel.

TABLE I
Main Characteristics of the PARSAX radar [51]

Category	Parameter	Value
System characteristics	Center frequency Modulation bandwidth Range resolution	3.315 GHz ≤ 100 MHz ≤ 1.5 m
Max. power (per TX channel)	High-power mode Low-power mode	100 W 0.2 W
TX parabolic antenna	Antenna diameter Antenna beamwidth Antenna gain	4.28 m 1.8° 40.0 dBi
RX parabolic antenna	Antenna diameter Antenna beamwidth Antenna gain	2.12 m 4.6° 32.8 dB
TX-RX isolation	HH-polarized VV-polarized	-100 dB -85 dB
ADC characteristics	Max. sampling frequency ADC resolution	400 MHz 14-b

low-power or high-power amplification stage. In the operating mode, this signal is radiated toward the search direction via the transmit antenna, and the signals backscattered from the environment are collected using the receiving antenna. In the calibration mode, the amplified probing signal is first attenuated and then directly sent to the RF receiver through a fixed-length delay line with known attenuation (see Fig. 2).

At the receiver side, after low noise amplification, frequency down-conversion to the intermediate frequency, and signal conditioning, the resulting signal is passed to the digital receiver. Within the receiver board, the received and reference signals are synchronously sampled via parallel analog-to-digital converters (ADCs) with a sampling rate of 400 MHz using a 14-b digital representation. Finally, the aforementioned sampled signals are sent to the field programmable gate array (FPGA), where different processing schemes can be loaded for real-time operation [50]. This can include deramping, matched filtering, or direct streaming mode that simply transfers the sampled signal to the computer for further processing. Table I summarizes the main characteristics of the PARSAX radar.

²The PAs are manufactured by Microwave Amplifiers Ltd. Specifically, an AM7-3.3S-22-30 is used in low-power mode, while an AM82-3.3S-27-50 is employed in high-power setup.

IV. EXPERIMENTAL ANALYSIS

In this study, the AWG of the PARSAX system is fed with digitally customized waveforms designed according to the method discussed in Section II. Specifically, leveraging the algorithm proposed in [19], spectrally notched waveforms are synthesized and their effectiveness assessed employing both calibration and operating modes. The analysis is conducted by considering the measurement configurations described as follows.

- Measurement Setup 1: the calibration mode is exploited to assess whether the spectral characteristics of the transmitted signals conform the spectral requirements forced at the design stage.
- 2) *Measurement Setup 2:* open-air experiments are conducted to prove the ability of the designed waveforms to detect both stationary and moving targets.
- 3) *Measurement Setup 3:* open-air experiments are conducted to demonstrate the spectral coexistence between the probing radar waveform and a frequency-overlaid communication signal.

The considered experiments involve the use of the lowpower mode, the high-power mode, or both. Besides, in the former configuration the amplifier operates in its linear region, while in the latter setting, it works in its compression region.

A. Measurement Setup 1

The waveform design algorithm in [19] assumes an ideal behavior of the components involved in the transmit chain of the radar system. However, as discussed in [47], possible hardware nonidealities (especially those related to the power amplification stage) may introduce spectral distortions in the actual waveform transmitted into the environment, potentially compromising the spectral compatibility requirement. For this reason, it is crucial to establish whether the radar system alters the characteristics of the designed waveform. This initial assessment is conducted by analyzing the signal gathered at the output of both the AWG and the amplification stage of the transmit chain using the feedback channel and calibration mode, respectively.

The spectrally notched waveform is designed using a linear up-chirp as the reference code, with a time duration of $50~\mu s$ and a frequency bandwidth of 40~MHz. Furthermore, the spectral mask specified during the design stage includes three frequency notches, characterized by a width of 2~MHz and a depth of 35~dB. In addition, the similarity parameter is set to 0.1.

After synthesizing the waveform, a train of uniformly spaced pulses with a pulse repetition time (PRT) of 200 μ s is formed and generated via the AWG of PARSAX. Subsequently, measurements are collected during the transmission of 512 pulses while the system is operated in high-power mode. In this regard, it is important to note that the signals from the feedback and receive channels undergo a synchronous sampling, triggered by the start epoch of the pulse train. This enables data segmentation into 512

TABLE II
Parameters Considered for Measurement
Setup 1

Parameter	Value
Pulse Width	$50 \mu s$
Bandwidth	40 MHz
PRT	$200~\mu s$
Number of processed pulses	512
Number of stop bands	3
Stop-bands width	2 MHz
Notches depth	35 dB
Similarity	0.1

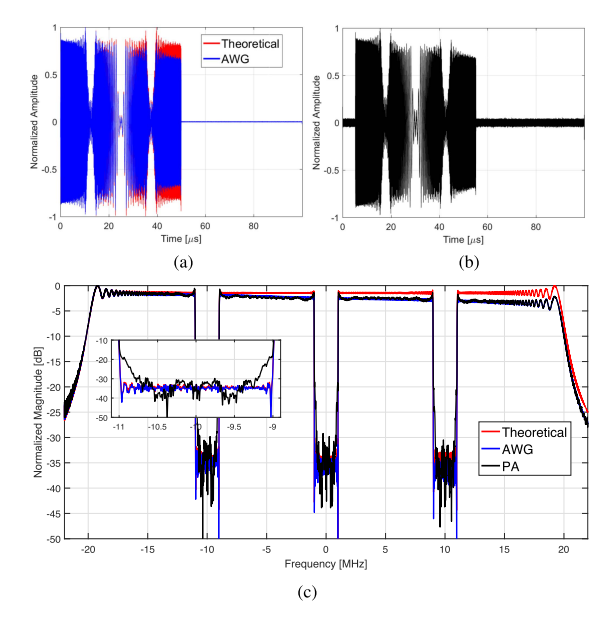


Fig. 3. Comparison between the theoretical waveform and the signals gathered using Measurement Setup 1 in the (a) and (b) time and the (c) frequency domain.

time intervals, each corresponding to one PRT. Table II summarizes the key parameters for this measurement setup.

As mentioned before, the analysis aims at verifying the similarity between the synthesized waveform (referred to as the theoretical signal) and the measured signals. The comparison is shown in both the time and frequency domains in Fig. 3.

Fig. 3(a) shows the real part³ of both the theoretical signal and the signals measured at the output of the AWG. Fig. 3(b), instead, displays the real part of the signals collected at the output of the amplification stage. Note that for both figures, the reported measured signals are those collected over each repetition interval of the generated pulse train (i.e., 512 overlapped signals). Moreover, since the transmitted pulses have a time duration of 50 μ s, the time axis is limited to 100 μ s (instead of considering the entire PRT of 200 μ s). Finally, both the theoretical and the measured signals are normalized with respect to their maximum value.

The comparison in Fig. 3(a) reveals a good agreement between the theoretical signal and the waveform generated

³The samples of the complex envelope are obtained through digital down-conversion.

using the AWG. However, an almost linear attenuation over the pulse extension of the measured data is clearly visible. As to the measurements performed after the amplification stage, Fig. 3(b) highlights that the collected signals can be considered delayed versions of the waveform generated using the AWG with a time offset matching the delay line length involved into the calibration mode.

Fig. 3(c) compares the average frequency spectra of the theoretical waveform and of the signals gathered downstream with the AWG and the power amplifification stage. The curves are obtained by averaging the frequency spectra evaluated using all the available 512 segments and then normalizing each frequency spectrum with respect to its maximum value. Since the reference code is a linear upchirp, the results certify that the linear attenuation observed in the time domain is reflected in the frequency domain as a linear attenuation from the low- to the high-frequency components of the collected signals. This attenuation only affects the amplitude of the generated signal and could be compensated with a suitable precalibration of the AWG. In fact, comparing the frequency spectrum of the waveform generated with the AWG with the theoretical counterpart reveals that no spectral distortions are present and the depth of the frequency notches remains almost unchanged.

As to the signal after the amplification stage, since transitions are observed at the edges of the frequency notches, the spectral requirements specified during the design stage (viz., the depth of the frequency notches) are tightly guaranteed only in correspondence of the center of the stop-band. Such spectral distortions can be attributed to the high-power amplification stage. Indeed, performing the same analysis in the low-power mode (not reported here for brevity), such transitions are not present, and the spectrum of the signal collected after the (low-power) amplification stage closely complies with the theoretical mask. Nevertheless, even though spectral distortions are present in the high-power setting, the addition of guard bands for each frequency notch could offer a viable solution to ensure the desired spectral requirements over the entire stop-bands of interest.

The final analysis aims at investigating whether the transmit and/or receive chains compromise the expected performance in terms of pulse compression. In this respect, the nominal output of the pulse compressor corresponds to a lagged version of the autocorrelation of the designed (theoretical) waveform, with a time lag equal to the delay introduced by the calibration line. This benchmark is compared with its measured counterpart, obtained by cross-correlating the data collected (after power amplification) through the calibration line across the available 512 data segments with a specific signal (representative of the assumed transmitted pulse) and then averaging the resulting 512 cross-correlation functions. In particular, the following three filters are considered:

- 1) theoretical spectrally notched signal;
- 2) spectrally notched signal downstream of the AWG;
- 3) spectrally notched signal downstream of the power amplification stage;

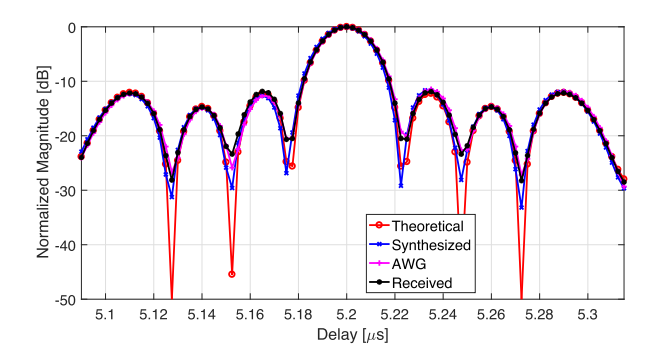


Fig. 4. Comparison between the theoretical and the actual cross-correlations for the signals gathered in Measurement Setup 1.

referred to hereafter as synthesized, AWG, and received, respectively. In the last two cases, leveraging knowledge about both the time duration of the spectrally notched pulse and the delay introduced by the calibration line, the filters for pulse compression are defined using samples acquired via the feedback channel (Case 2) and the receive channel (Case 3) across the first of the 512 available data segments.

The results of the analysis are shown in Fig. 4 where the modulus of the averaged cross-correlations is compared with the theoretical benchmark. The curves highlight that all the considered cross-correlation functions exhibit a peak corresponding to the nominal delay introduced by the calibration line. Furthermore, when comparing the theoretical benchmark with the measured counterparts, only a change in the nulls' depth is observed. More in detail, the main lobe width and the sidelobe levels remain almost unaltered, indicating that neither the AWG nor the power amplifier of the PARSAX affect the expected radar performance in terms of pulse compression.

B. Measurement Setup 2

This section presents the results of open-air experiments where the radar waveform considered for Measurement Setup 1 (with parameters specified in Table II) is radiated into the environment. The PARSAX radar is operated in single polarization mode, specifically with the horizontal polarization in both transmission and reception, and in low power mode to avoid saturation of the receiver channel. Hence, data are collected in two scenarios as detailed in the following.

- 1) Scenario 1 (Single Target of Opportunity): the radar is pointed toward a stationary target of opportunity located at approximately 1.14 km. This target is a tall chimney, made of four colocated cylindrical pipes, as in Fig. 5(a).
- 2) Scenario 2 (Multiple Moving Targets of Opportunity): the radar is pointed toward a highway segment located at approximately 4.02 km, as shown in the maps of Fig. 5(b). This setup allows to test the radar performance in the presence of multiple moving targets of opportunity, i.e., uncooperative vehicles driving along the two directions of the highway.

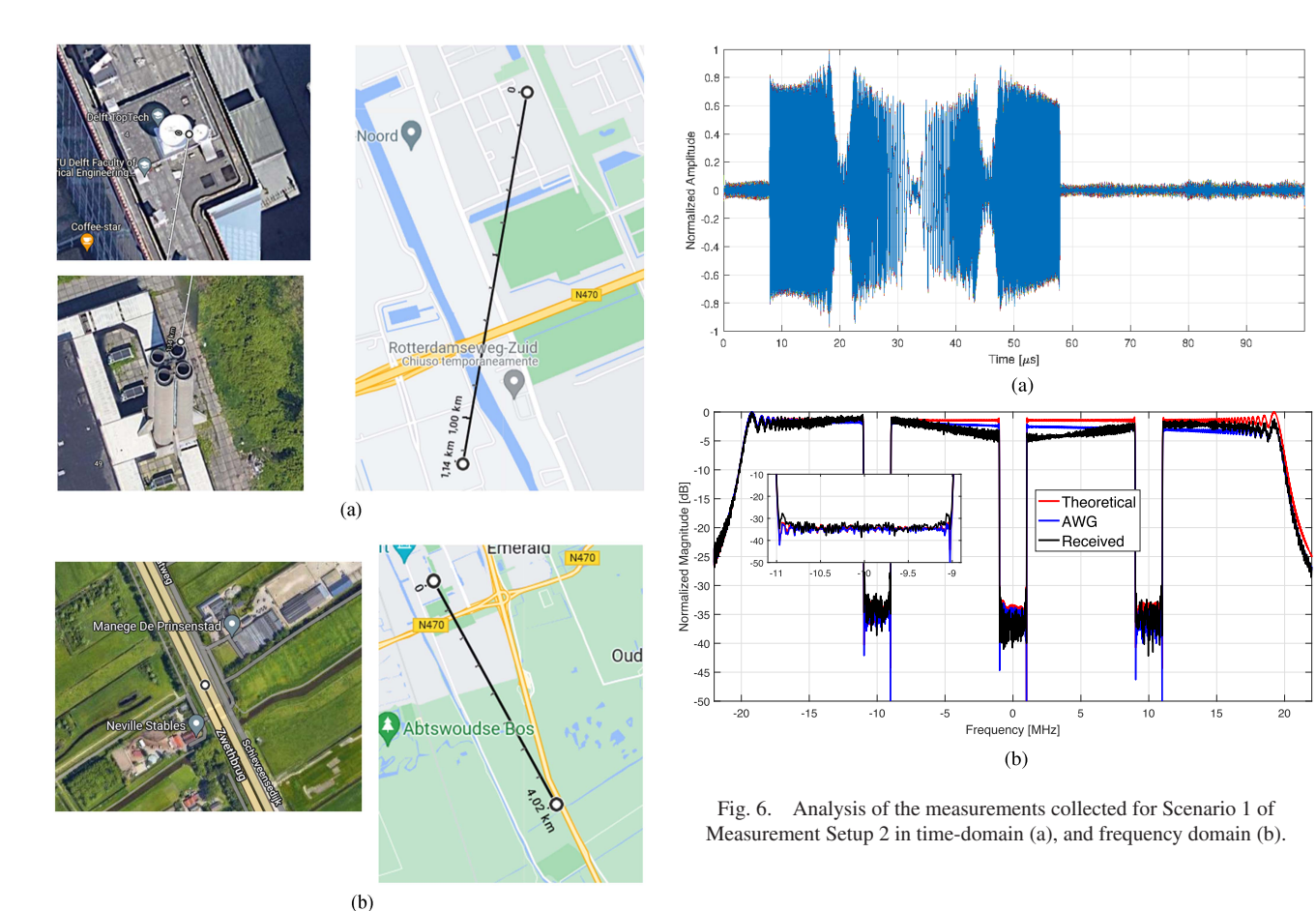


Fig. 5. Scenarios for the Measurement Setup 2: Scenario 1 with a stationary target of opportunity (a), and Scenario 2 with multiple moving targets of opportunity (b).

In both the situations, the signals backscattered from the environment are collected and analyzed considering a coherent processing interval (CPI) composed of 512 pulses. Before discussing the results, it is worth pointing out that the PARSAX system uses two distinct antennas for simultaneous transmission and reception, thus enabling short-distance detection without eclipsing ranges.

The first analysis is focused on determining whether the probing signal complies with the spectral requisites forced at the design stage. This study is conducted using the signals backscattered from the environment of Scenario 1, which mainly involves a chimney located at a relatively short range. Given the narrow beam of the transmit antenna and the high RCS of the target, it is expected that the received signals are just delayed copies of the probing waveform, with a time elapse proportional to the range of the target. The results of this assessment are displayed in Figs. 6 in both time and frequency domains (using the same normalizations as for the analysis in Measurement Setup 1). Precisely, Fig. 6(a) shows the real part of the collected signals, while Fig. 6(b) compares the average frequency spectrum of the generated and received signals with the theoretical counterpart. The time-domain analysis confirms that the received signals can be viewed as delayed versions of the transmitted waveform, whose delay matches the range of the chimney. The frequency spectrum curves show that the depth of the frequency notches remains almost unchanged, indicating that the probing signal satisfies the spectral constraints set during the design stage.

For Scenario 2, the analysis of the acquired signals in both time and frequency domains is illustrated in Fig. 7(a) and (b), respectively. As mentioned before, this study case accounts for multiple moving targets on a highway segment located approximately 4-km away from the radar. This is reflected in the complex structure of the signals received during the CPI, as compared with those collected for Scenario 1; see Figs. 6(a) and 7(a). Nonetheless, Fig. 7(b) indicates that the depth of the frequency notches in the stop-bands still fulfils the spectral constraints set to ensure the compatibility between the probing waveform and the external electromagnetic environment. Notably, since for both the scenarios the measurements are performed using the low-power mode, no transitions are present at the edges of the frequency notches. This behavior is consistent with the results discussed in Section IV-A for Measurement Setup 1. In other words, no spectral distortions are induced on the probing radar waveform, and the frequency spectrum of the transmitted signal closely adheres with the theoretical mask specified at the design stage.

The next study addresses the capability of the designed spectrally notched waveform to detect the targets present in the considered scenarios using as figure of merit range profiles and the range-Doppler maps. The range profiles

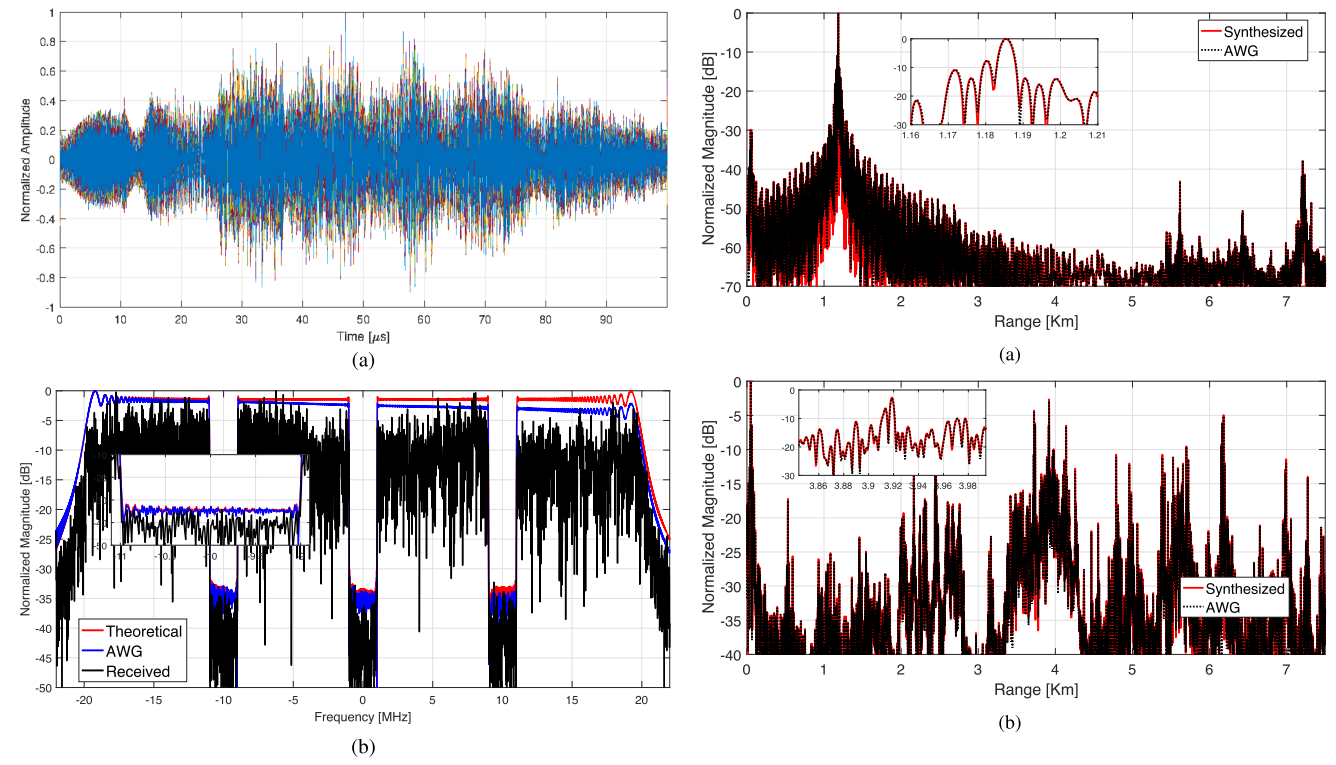


Fig. 7. Analysis of the measurements collected for Scenario 2 of Measurement Setup 2 in time-domain (a), and frequency domain (b).

are obtained by performing pulse compression and non-coherent integration over the pulses gathered during the CPI. In this respect, matched filtering operation for pulse compression is realized using both the theoretical waveform and the waveforms generated via the AWG for each pulse of the pulse train. The resulting range profiles are hereafter referred to as synthesized and AWG, respectively. The range-Doppler maps, instead, are obtained by performing standard pulse-Doppler processing over the samples in the slow-time domain after pulse compression.

Regardless of the filter used for pulse compression, the curves in Fig. 8 highlight that nearly identical range profiles are obtained in each of the considered scenarios. Moreover, the plot of Fig. 8(a) for Scenario 1 shows, as expected, a prominent peak at the nominal distance of the chimney. The range profiles in Fig. 8(b) for Scenario 2, instead, exhibit a more intricate shape than the former case, suggesting the presence of multiple targets.

Finally, the range-Doppler map in Fig. 9(a) for Scenario 1 corroborates the presence of a single stationary target (zero-Doppler) whose range matches the distance of the chimney. For Scenario 2, Fig. 9(b) indicates the presence of both stationary and moving targets. This is because, given the transmit and receive antenna beam sizes, even if the radar is pointed to the highway segment, the radar also illuminates and receives echoes from other objects in the environment, such as buildings and vegetation. Besides, when examining ranges corresponding to the illuminated highway segment, the map reveals the presence of multiple scatterers approaching and receding from the radar, whose

Fig. 8. Range profile after pulse compression applying noncoherent integration for scenario 1 (a), and scenario 2 (b).

ranges and velocities consistent with those of the vehicles traveling along a highway.

Summarizing, the presented analysis reveal that for both scenarios the probing radar signal complies with the spectral requisites set at the design stage to ensure spectral coexistence. Furthermore, the range profiles and range-Doppler maps demonstrate the capability of the system to detect both stationary and moving targets using the designed spectrally notched waveform.

C. Measurement Setup 3

In this section, the capability of the considered algorithm to synthesize waveforms ensuring spectral coexistence with frequency-overlaid signals is evaluated focusing on the communication system side. This assessment requires the following operations.

- The simultaneous transmission into the environment of a properly designed spectrally notched radar waveform and a communication signal in the same frequency band.
- 2) The measurement of the total signal within the frequency band of interest.
- 3) The evaluation of the error rate in decoding the communication signal at the receiving site.

As explained in Section III, the PARSAX is a fully polarimetric SDR system. Hence, the transmission task can be accomplished via the cross-polarized transmit channels, whereas the reception task is accomplished by an RF receiver equipped with a 45° linearly polarized antenna. For the conducted experiments the signals transmitted via the

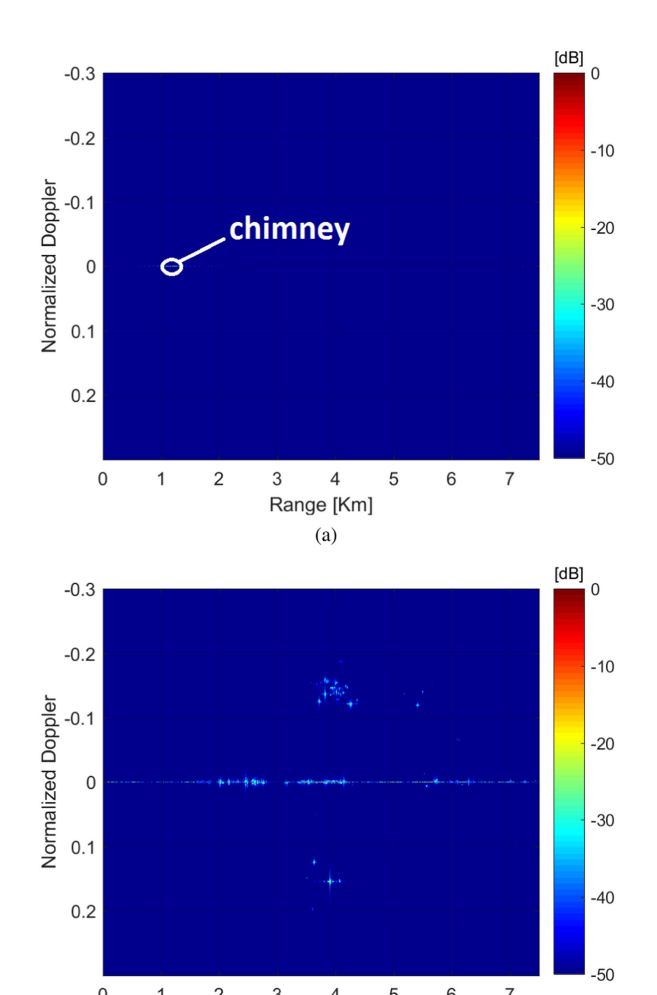


Fig. 9. Range-Doppler maps for (a) scenario 1 with stationary target of opportunity and (b) scenario 2 with multiple moving targets.

Range [Km] (b)

H and V channels of the PARSAX (i.e., the radar and communication signals, respectively) are collected using a PlutoSDR [52]. This is a software-defined-radio transceiver manufactured by Analog Devices and is capable of receiving signals in the frequency range from 70 MHz–6 GHz. It offers an instantaneous bandwidth up to 20 MHz, supports a sampling frequency up to 61.44 MHz, and provides the complex envelope of the received signal. More in detail, the PlutoSDR is positioned on the roof of a building located approximately 300-m away from the radar system.

Fig. 10 provides an overview of the measurement setup, whereas Fig. 11(a) and (b) depict the PARSAX system pointed toward the RF receiver. Fig. 11(c), instead, illustrates the PARSAX as it is seen from the receiver side.

The analysis is conducted by transmitting two data signals modulated according to a $\pi/4$ differential quadrature phase-shift keying (DQPSK) scheme (denoted as e_1 and e_2 in the following), each occupying an RF bandwidth of 200 KHz. The $\pi/4$ -DQPSK is a digital modulation technique in which the data bit stream is mapped into a sequence of symbols, each carrying two bits of information. Differently from the classic phase-shift keying (PSK)



Fig. 10. Measurement setup involving the simultaneous transmission and reception of the spectrally-notched radar waveform and the communication signals.

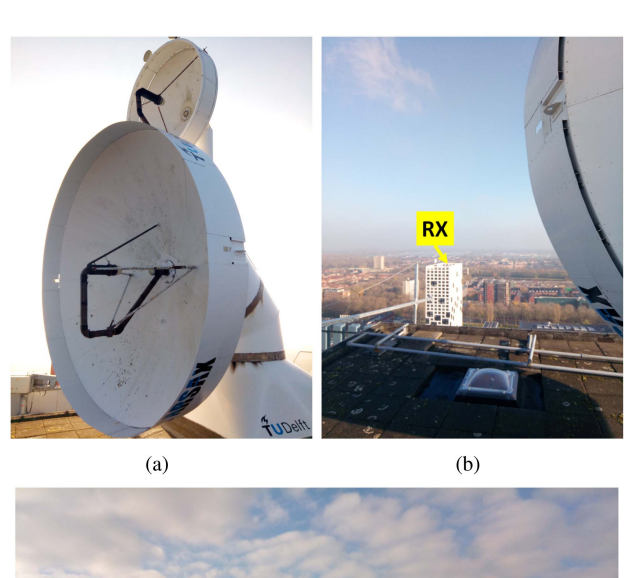




Fig. 11. (a) PARSAX transmit antenna pointed towards the receiver which is shown in (b), and (c) PARSAX as it is seen from the receiver side.

modulation scheme, where each symbol is modulated via a specific phase value, in $\pi/4$ -DQPSK, the current modulation symbol is obtained by applying a phase transition to the previous modulation symbol, which can take values of $\pi/4$, $3\pi/4$, $-\pi/4$, or $-3\pi/4$ to encode the bit pairs 00, 01, 10, 11, respectively.

For the conducted experiments, the overall communication signal is generated as $e = e_1 + e_2$, where e_1 and e_2 are orthogonal in the frequency domain and exhibit a frequency

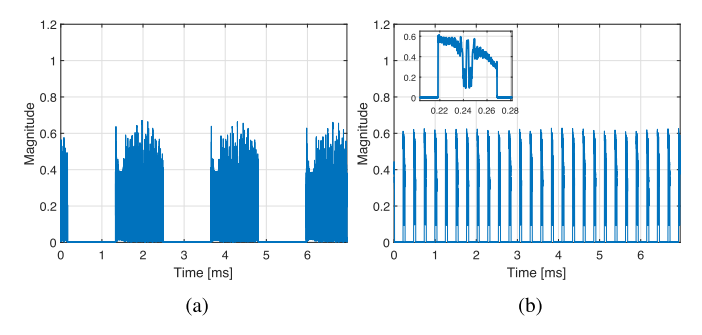


Fig. 12. Time-domain behavior of the reference measurements for (a) the communication signals and (b) the spectrally notched radar waveform

offset of 1 MHz. As to the spectrally notched radar waveform (denoted as s in the following), this is synthesized using as reference code a linear down-chirp pulse whose width is 50 μ s and whose bandwidth is 10 MHz. Moreover, to account for the presence of e_1 and e_2 , two stop bandwidths are forced at the design stage whose width and depth are 450 KHz and -35 dB, respectively.

After synthesizing the radar code s and generating the communication signal e, they are used to form bursts with PRT of 200 μ s and 1 ms, respectively. Subsequently, the former is transmitted using the H channel at the carrier frequency of the PARSAX system, namely $f_c = 3.315$ GHz. The latter is transmitted using the V channel so that the carrier frequencies of e_1 and e_2 are 3.3145 and 3.3155 GHz, respectively (i.e., $f_c \pm 500$ KHz).

Leveraging the capability of the PARSAX to introduce distinct attenuation levels over each transmit channel, the performance is evaluated under diverse signal-to-interference ratio (SIR) conditions. Precisely, using the high-power mode for both the H and V channels, the following case studies are considered:

- 1) $\kappa_s = 0 \text{ dB}, \kappa_e = 0 \text{ dB};$
- 2) $\kappa_s = 0 \text{ dB}, \kappa_e = 10 \text{ dB};$
- 3) $\kappa_s = 0 \text{ dB}, \kappa_e = 20 \text{ dB};$
- 4) $\kappa_s = 0 \text{ dB}, \kappa_e = 30 \text{ dB};$

where κ_s and κ_e denote the attenuation levels introduced on s and e, respectively. For reference, measurements are acquired under three conditions: 1) transmission of only s with $\kappa_s = 0$ dB; 2) transmission of only e with $\kappa_e = 0$ dB; and 3) no active transmissions from the PARSAX system. These measurements are used both for comparison purposes and to evaluate the SIR in the shared frequency bands for each case study. Notably, all the acquisitions are performed without employing automatic gain control, while manually regulating the dynamic range of the receiver so as to prevent clipping of the collected signals under the Case 1 (providing he maximum received power).

Figs. 12 and 13 display the time-domain behavior of the signals gathered over an acquisition window of approximately 7 ms for the reference measurements and all the case studies, respectively. As to the reported amplitude values, the PlutoSDR provides digitized signals normalized within

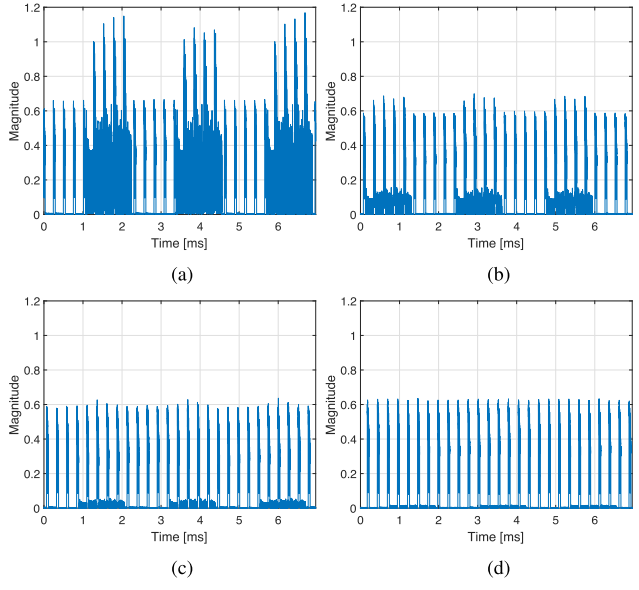


Fig. 13. Time-domain behavior of the signals collected for (a) Case 1, (b) Case 2, (c) Case 3, and (d) Case 4.

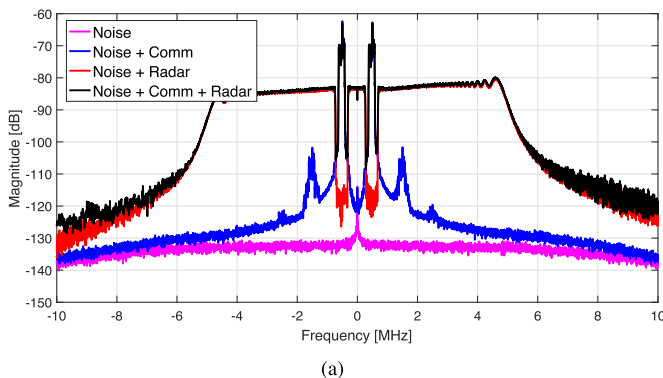
the interval [-1, 1]. Converting these values in standard units, such as volts, requires information about the technical specifications of the ADC and this is beyond the scope of this study.

Fig. 12 highlights that when $\kappa_s = \kappa_e$, the 45° linearly polarized receiving antenna ensures nearly identical peak amplitudes for the signals transmitted via the cross-polarized channels of the PARSAX system. In addition, as in the previous experiments, the transmitted radar waveform exhibits a linear attenuation along its pulse duration. The plots in Fig. 13, instead, highlight that while the peak amplitudes associated with *s* are nearly identical for all the considered case studies, those associated with *e* progressively decrease from Cases 1 to 4.

Fig. 14 depicts the frequency spectrum of the reference measurements along with that of the signals collected for Case 1 (where $\kappa_s = \kappa_e = 0$ dB as in the reference scenarios). The reported curves highlight that:

- 1) the dominant spectral components of the reference data almost overlap with those of the signal acquired for Case 1, where both *s* and *e* are transmitted simultaneously;
- the frequency spectrum of the reference communication waveform reveals the presence of spurious signals, likely due to nonidealities in the transmit/receive chain (this will be subject to further investigation in the future);
- 3) the depth of the frequency notches meets the spectral requirements set during the design stage;
- 4) the probing radar waveform exhibits a linear attenuation from high- to low-frequency components.

Since the reference code is a linear down-chirp, the latter trend is compliant with the linear attenuation in the time domain observed in Fig. 12(b).



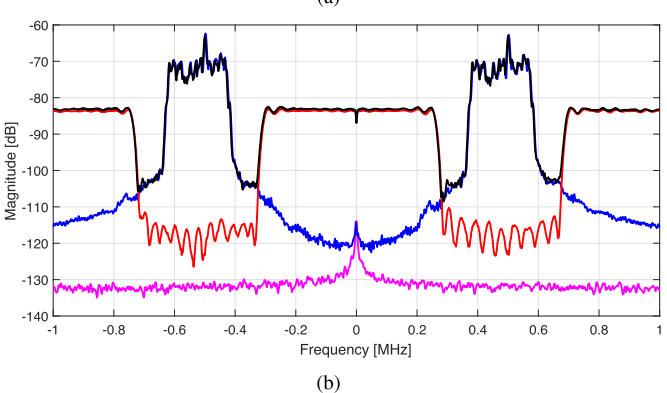


Fig. 14. Frequency-domain behavior of both (a) the reference measurements and the signals collected for Case 1 and (b) a zoomed-in view in correspondence of the stop bandwidths.

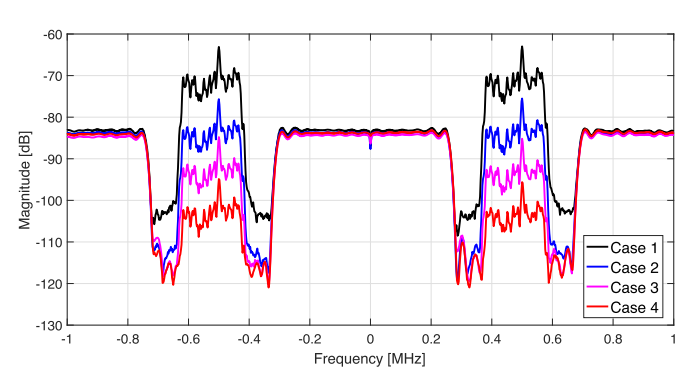


Fig. 15. Zoomed-in view of the frequency spectra of the acquired signals from Cases 1 to 4 in correspondence of the stop bandwidths.

Besides, the frequency spectra evaluated using the measurements gathered for all the considered case studies shown in Fig. 15 highlight that moving from Cases 1 to 4:

- the spectral components corresponding to the communication signal are progressively attenuated according to a factor of about 10 dB;
- 2) the frequency components related to the radar code remain almost unchanged.

The next analysis concentrates on the evaluation of the SIR, which is formally defined as

$$SIR = \frac{P_e}{P_s}$$

TABLE III
Average SIR Values (In
dB) Experienced in
Each Communication
Channel

Case	e_1	e_2
1	47.8	47.5
2	36.9	36.6
3	26.7	26.0
4	15.2	14.3

where P_e and P_s are the power levels of the communication and radar signals in a given shared frequency band, respectively.

As mentioned before, the spectral characteristics of both the radar waveform and the receiver noise remain unaltered across the reference collection and the considered case studies. Hence, the aforementioned power levels can be estimated as

$$\hat{P}_e = \hat{P}_r - \hat{P}_s^{\mathrm{ref}}$$
 $\hat{P}_s = \hat{P}_s^{\mathrm{ref}} - \hat{P}_n^{\mathrm{ref}}$

where, for a given shared frequency band:

- 1) \hat{P}_r indicates the average power calculated using the signals collected for a particular case study, encompassing contributions from e, s, and receiver noise;
- 2) \hat{P}_s^{ref} denotes the average power calculated using the radar waveform reference measurements, accounting for contributions from s and receiver noise;
- 3) \hat{P}_n^{ref} is the average noise power calculated using the noise reference measurements.

Table III provides the SIR experienced in each shared frequency band averaged over 100 acquisition windows. The reported values demonstrate that:

- 1) for each case study, the SIRs over the two shared frequency band are nearly identical;
- 2) moving from Cases 1 to 4, where κ_s remains constant and κ_e progressively decreases by 10 dB, the SIR also diminishes progressively by approximately 10 dB.

The effectiveness of the waveform design in ensuring spectral coexistence is further assessed by examining the average error rate experienced in each communication channel. Precisely, within each acquisition window, the received communication signals (of a given pulse) for both emitters are demodulated, and decoded. Subsequently, the decoded information bit sequences associated with e_1 and e_2 (each composed of 368 b) are compared with their respective nominal counterparts, and the empirical error rate is evaluated. Table IV presents the error rates averaged over 100 acquisition windows.

The values clearly indicate that the communication links are not significantly compromised by the radar probing waveform, thereby demonstrating coexistence among these systems. In addition, the average error rates tend to increase as the SIR decreases. As an additional remark it is worth

TABLE IV Average Error Rate (In %) Experienced in Each Communication Channel

Case	e_1	e_2
1	0	0
2	0	0
3	0	0
4	0.56 %	0.49 %

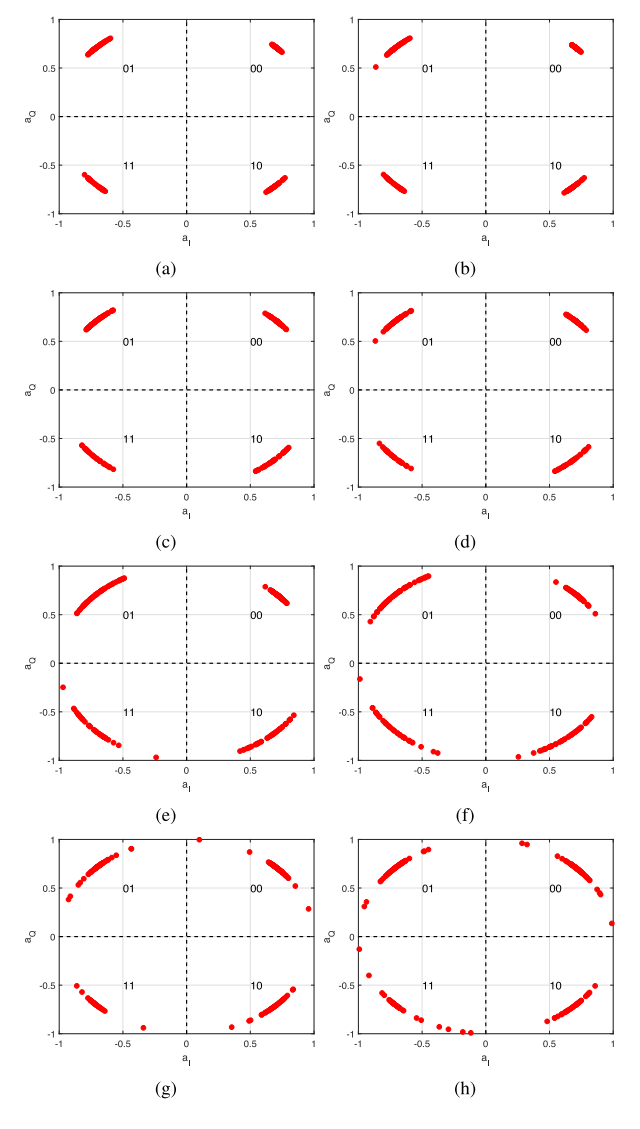


Fig. 16. Scatterplot of phase transitions between consecutive symbols for a single communication signal, evaluated for each emitter and case study: (a) Case 1/e₁, (b) Case 1/e₂, (c) Case 2/e₁, (d) Case 2/e₂, (e) Case 3/e₁, (f) Case 3/e₂, (g) Case 4/e₁, and (h) Case 4/e₂.

mentioning that, besides the SIR, other factors also contribute to possible errors, including synchronization issues. Specifically, more sophisticated synchronization algorithms and the use of error correction schemes could potentially help to reduce the error rate.

Finally, Fig. 16 shows a scatterplot of phase transitions between consecutive symbols of a single communication pulse, evaluated for each emitter and case study. Here, for a given phase transition θ_d , $a_I = \cos(\theta_d)$, and $a_Q = \sin(\theta_d)$.

The plots emphasize that the dispersion around the true value of the estimated phase transitions increases as the SIR decreases, as predicted by the average error rates shown in Table IV.

V. CONCLUSION

This article has dealt with the experimental validation of waveforms designed leveraging the algorithm proposed in [19], enabling radars to operate in spectrally crowded environments. The study has been conducted through a measurement campaign involving the use of the PARSAX system, a fully polarimetric *S*-band SDR located at TU Delft, in The Netherlands.

First, an overview of the waveform design strategy considered to ensure coexistence among the radar and other RF systems operating in the same frequency interval has been provided. Then, the main features of the PARSAX system have been summarized, with an emphasis on its calibration and sensing operational modes, as well as on the availability of either a low-power (0.2 W) or a high-power (100 W) amplifier at the transmit side.

As to the experimental analysis, it has been carried out by forming trains of uniformly spaced spectrally notched pulses and by feeding the AWG of the PARSAX radar with the corresponding digital samples.

The capabilities of the considered signals in ensuring spectral coexistence, as well as to detect both stationary and moving targets, have been evaluated employing specific measurement setups. Precisely, the compliance between the signals produced by PARSAX, downstream of both the AWG and the power amplification stage, and the designed waveforms, has been first studied using feedback channels available in the SDR system (Measurement Setup 1). Subsequently, the system's ability to detect targets has been investigated by radiating the spectrally notched probing signal into the environment and analyzing the echoes backscattered from the illuminated scene (Measurement Setup 2). Finally, spectral coexistence has been assessed by simultaneously radiating the designed waveform and a frequency-overlaid communication signal into the environment, so as to verify whether the interference produced by the radar in the shared frequency bands compromises the communication link (Measurement Setup 3).

The conducted experimental analysis has demonstrated that the considered spectrally notched probing signals once transmitted into the environment meet the requirements specified at the design stage to ensure spectral coexistence and at the same time enable the system to detect both stationary and moving targets.

Future research directions might focus on exploring the transmission of the signals using a phased-array radar. In addition, it is definitely of interest to study the integration of a spectrum sensing module into the probing system to gather online spectrum awareness from the environment and realize the so-called perception-action cycle in the context of cognitive radars.

- [1] H. Griffiths et al., "Radar spectrum engineering and management: Technical and regulatory issues," *Proc. IEEE*, vol. 103, no. 1, pp. 85–102, Jan. 2015.
- [2] S. Blunt and E. Perrins, Radar and Communication Spectrum Sharing, (Radar, Sonar and Navigation). London, U.K.: Inst. Eng. Technol., 2018.
- [3] R. Klemm, U. Nickel, C. Gierull, P. Lombardo, H. Griffiths, and W. Koch, Novel Radar Techniques and Applications Volume 2: Waveform Diversity and Cognitive Radar, and Target Tracking and Data Fusion, (Radar, Sonar & Navigation), Raleigh, NC, USA: SciTech, vol. 2, 2017. [Online]. Available: https://shop.theiet.org/novel-radartech-apps-vol-2
- [4] B. Paul, A. R. Chiriyath, and D. W. Bliss, "Survey of RF communications and sensing convergence research," *IEEE Access*, vol. 5, pp. 252–270, 2017.
- [5] L. Zheng, M. Lops, Y. C. Eldar, and X. Wang, "Radar and communication coexistence: An overview: A review of recent methods," *IEEE Signal Process. Mag.*, vol. 36, no. 5, pp. 85–99, Sep. 2019.
- [6] F. Liu et al., "Seventy years of radar and communications: The road from separation to integration," *IEEE Signal Process. Mag.*, vol. 40, no. 5, pp. 106–121, Jul. 2023.
- [7] C. Zhang et al., "Slow-time ambiguity function shaping with spectral coexistence for cognitive radar," *IEEE J. Sel. Topics Appl. Earth Observ. Remote Sens.*, vol. 16, pp. 8418–8430, 2023.
- [8] M. Wicks, "Spectrum crowding and cognitive radar," in *Proc. 2nd Int. Workshop Cogn. Inf. Process.*, 2010, pp. 452–457.
- [9] A. Farina, A. De Maio, and S. Haykin, *The Impact of Cognition on Radar Technology (Radar, Sonar and Navigation)*. London, U.K.: Inst. Eng. Technol., 2017.
- [10] J. Guerci, Cognitive Radar: The Knowledge-Aided Fully Adaptive Approach, 2nd Ed. Norwood, MA, USA: Artech, US, 2020.
- [11] S. Haykin, "Cognitive radar: A way of the future," *IEEE Signal Process. Mag.*, vol. 23, no. 1, pp. 30–40, Jan. 2006.
- [12] M. S. Greco, F. Gini, P. Stinco, and K. Bell, "Cognitive radars: On the road to reality: Progress thus far and possibilities for the future," *IEEE Signal Process. Mag.*, vol. 35, no. 4, pp. 112–125, Jul. 2018.
- [13] S. Z. Gurbuz, H. D. Griffiths, A. Charlish, M. Rangaswamy, M. S. Greco, and K. Bell, "An overview of cognitive radar: Past, present, and future," *IEEE Aerosp. Electron. Syst. Mag.*, vol. 34, no. 12, pp. 6–18, Dec. 2019.
- [14] A. F. Martone, K. I. Ranney, K. Sherbondy, K. A. Gallagher, and S. D. Blunt, "Spectrum allocation for noncooperative radar coexistence," *IEEE Trans. Aerosp. Electron. Syst.*, vol. 54, no. 1, pp. 90–105, Feb. 2018.
- [15] A. Aubry, V. Carotenuto, A. De Maio, and M. A. Govoni, "Multi-snapshot spectrum sensing for cognitive radar via blocksparsity exploitation," *IEEE Trans. Signal Process.*, vol. 67, no. 6, pp. 1396–1406, Mar. 2019.
- [16] A. F. Martone et al., "Closing the loop on cognitive radar for spectrum sharing," *IEEE Aerosp. Electron. Syst. Mag.*, vol. 36, no. 9, pp. 44–55, Sep. 2021.
- [17] J. A. Kovarskiy, A. F. Martone, R. M. Narayanan, and K. D. Sherbondy, "Restless bandits for metacognitive spectrum sharing with software defined radar," *IEEE Trans. Radar Syst.*, vol. 1, pp. 401–412, 2023.
- [18] R. G. Mattingly and J. G. Metcalf, "Fast adaptive spectrum sensing using hardware optimized, cell averaging estimation for cognitive radio and radar applications," *IEEE Trans. Aerosp. Electron. Syst.*, vol. 59, no. 5, pp. 5084–5096, Oct. 2023.
- [19] A. Aubry, V. Carotenuto, and A. D. Maio, "Forcing multiple spectral compatibility constraints in radar waveforms," *IEEE Signal Process. Lett.*, vol. 23, no. 4, pp. 483–487, Apr. 2016.
- [20] A. Aubry, V. Carotenuto, A. De Maio, A. Farina, and L. Pallotta, "Optimization theory-based radar waveform design for spectrally dense environments," *IEEE Aerosp. Electron. Syst. Mag.*, vol. 31, no. 12, pp. 14–25, Dec. 2016.

- [21] A. Aubry, A. De Maio, M. A. Govoni, and L. Martino, "On the design of multi-spectrally constrained constant modulus radar signals," *IEEE Trans. Signal Process.*, vol. 68, pp. 2231–2243, 2020.
- [22] S. D. Blunt, M. Cook, J. Jakabosky, J. De Graaf, and E. Perrins, "Polyphase-coded FM (PCFM) radar waveforms, Part I: Implementation," *IEEE Trans. Aerosp. Electron. Syst.*, vol. 50, no. 3, pp. 2218–2229, Jul. 2014.
- [23] S. D. Blunt, J. Jakabosky, M. Cook, J. Stiles, S. Seguin, and E. L. Mokole, "Polyphase-coded FM (PCFM) radar waveforms, Part II: Optimization," *IEEE Trans. Aerosp. Electron. Syst.*, vol. 50, no. 3, pp. 2230–2241, Jul. 2014.
- [24] B. Tang and J. Liang, "Efficient algorithms for synthesizing probing waveforms with desired spectral shapes," *IEEE Trans. Aerosp. Electron. Syst.*, vol. 55, no. 3, pp. 1174–1189, Jun. 2019.
- [25] H. He, P. Stoica, and J. Li, "Waveform design with stopband and correlation constraints for cognitive radar," in *Proc. 2nd Int. Workshop Cogn. Inf. Process.*, 2010, pp. 344–349.
- [26] Y. Huang, M. Piezzo, V. Carotenuto, and A. De Maio, "Radar waveform design under similarity, bandwidth priority, and spectral coexistence constraints," in *Proc. IEEE Radar Conf.*, 2017, pp. 1142–1147.
- [27] K. Alhujaili, X. Yu, G. Cui, and V. Monga, "Spectrally compatible MIMO radar beampattern design under constant modulus constraints," *IEEE Trans. Aerosp. Electron. Syst.*, vol. 56, no. 6, pp. 4749–4766, Dec. 2020.
- [28] Q. Lu, G. Cui, X. Yu, S. Chen, H. Kuang, and L. Kong, "Cognitive waveform design with desired spectrum-autocorrelation properties," *Signal Process.*, vol. 198, 2022, Art. no. 108576.
- [29] C.-W. Huang, L.-F. Chen, and B. Su, "Waveform design for optimal PSL under spectral and unimodular constraints via alternating minimization," *IEEE Trans. Signal Process.*, vol. 71, pp. 2518–2531, 2023.
- [30] J. W. Owen, P. M. McCormick, C. C. Jones, and S. D. Blunt, "On the optimality of spectrally notched radar waveform & filter designs," in *Proc. IEEE Radar Conf.*, 2023, pp. 1–6.
- [31] D. Salami, W. Ning, K. Ruttik, R. Jäntti, and S. Sigg, "A joint radar and communication approach for 5G NR using reinforcement learning," *IEEE Commun. Mag.*, vol. 61, no. 5, pp. 106–112, May 2023.
- [32] J. Owen, C. Mohr, B. Ravenscroft, S. Blunt, B. Kirk, and A. Martone, "Real-time experimental demonstration and evaluation of open-air sense-and-notch radar," in *Proc. IEEE Radar Conf.*, 2022, pp. 1–6.
- [33] J. W. Owen et al., "Experimental demonstration of cognitive spectrum sensing notching for radar," in *Proc. IEEE Radar Conf.*, 2018, pp. 0957–0962.
- [34] M. Alaee-Kerahroodi, E. Raei, S. Kumar, and B. S. M. R. R., "Cognitive radar waveform design and prototype for coexistence with communications," *IEEE Sensors J.*, vol. 22, no. 10, pp. 9787–9802, May 2022.
- [35] B. Ravenscroft, J. W. Owen, J. Jakabosky, S. D. Blunt, A. F. Martone, and K. D. Sherbondy, "Experimental demonstration and analysis of cognitive spectrum sensing and notching for radar," *IET Radar, Sonar Navigation*, vol. 12, no. 12, pp. 1466–1475, 2018.
- [36] G. E. Smith et al., "Experiments with cognitive radar," *IEEE Aerosp. Electron. Syst. Mag.*, vol. 31, no. 12, pp. 34–46, Dec. 2016.
- [37] G. E. Smith, "Cognitive radar experiments at the Ohio State University," in *Proc. Cogn. Commun. Aerosp. Appl. Workshop*, 2017, pp. 1–5.
- [38] S. W. Frost, B. Rigling, L. Patton, L. L. Monte, and B. Himed, "Experimental validation of sparse-frequency waveforms for congested spectrums," in *Proc. Int. Waveform Diversity Des. Conf.*, 2012, pp. 070–073.
- [39] S. A. Seguin, J. Jakabosky, and S. D. Blunt, "Hardware-in-the-loop radar waveform optimization using radiated emissions," in *Proc. IEEE Int. Symp. Electromagn. Compat.*, 2013, pp. 82–86.
- [40] C. P. Horne, J. Brown, G. E. Smith, A. E. Mitchell, and H. D. Griffiths, "Experimental spectral coexistence investigation for cognitive radar," in *Proc. Int. Conf. Radar Syst.*, 2017, pp. 1–6.

- [41] B. H. Kirk, R. M. Narayanan, K. A. Gallagher, A. F. Martone, and K. D. Sherbondy, "Avoidance of time-varying radio frequency interference with software-defined cognitive radar," *IEEE Trans. Aerosp. Electron. Syst.*, vol. 55, no. 3, pp. 1090–1107, Jun. 2019.
- [42] B. H. Kirk, K. A. Gallagher, J. W. Owen, R. M. Narayanan, A. F. Martone, and K. D. Sherbondy, "Cognitive software defined radar: A reactive approach to RFI avoidance," in *Proc. IEEE Radar Conf.*, 2018, pp. 0630–0635.
- [43] C. Baylis, M. Fellows, L. Cohen, and R. J. Marks II, "Solving the spectrum crisis: Intelligent, reconfigurable microwave transmitter amplifiers for cognitive radar," *IEEE Microw. Mag.*, vol. 15, no. 5, pp. 94–107, Jul./Aug. 2014.
- [44] L. Ryan, J. Jakabosky, S. D. Blunt, C. Allen, and L. Cohen, "Optimizing polyphase-coded FM waveforms within a LINC transmit architecture," in *Proc. IEEE Radar Conf.*, 2014, pp. 835–839.
- [45] A. Aubry, V. Carotenuto, A. De Maio, M. A. Govoni, and A. Farina, "Experimental analysis of block-sparsity-based spectrum sensing techniques for cognitive radar," *IEEE Trans. Aerosp. Electron. Syst.*, vol. 57, no. 1, pp. 355–370, Feb. 2021.
- [46] V. Carotenuto, A. Aubry, A. De Maio, N. Pasquino, and A. Farina, "Assessing agile spectrum management for cognitive radar on measured data," *IEEE Aerosp. Electron. Syst. Mag.*, vol. 35, no. 6, pp. 20–32, Jun. 2020.
- [47] A. Aubry, V. Carotenuto, A. De Maio, A. Farina, A. Izzo, and R. Schiano Lo Moriello, "Assessing power amplifier impairments and digital predistortion on radar waveforms for spectral coexistence," *IEEE Trans. Aerosp. Electron. Syst.*, vol. 58, no. 1, pp. 635–650, Feb. 2022.
- [48] V. Carotenuto et al., "Experimental evaluation of radar waveforms for spectral coexistence using the PARSAX radar," in *Proc. IEEE* 10th Int. Workshop Metrol. AeroSpace, 2023, pp. 389–394.
- [49] O. A. Krasnov, L. P. Ligthart, Z. Li, P. Lys, and F. van der Zwan, "The PARSAX - full polarimetric FMCW radar with dual-orthogonal signals," in *Proc. Eur. Radar Conf.*, 2008, pp. 84–87.
- [50] Z. Wang, O. A. Krasnov, G. P. Babur, L. P. Ligthart, and F. van der Zwan, "Reconfigurable digital receiver for polarimetric radar with dual-orthogonal signals," in *Proc. 7th Eur. Radar Conf.*, 2010, pp. 332–335.
- [51] O. A. Krasnov, G. P. Babur, Z. Wang, L. P. Ligthart, and F. van der Zwan, "Basics and first experiments demonstrating isolation improvements in the agile polarimetric FM-CW radar–PARSAX," *Int. J. Microw. Wireless Technol.*, vol. 2, no. 3/4, pp. 419–428, 2010.
- [52] T. Collins, R. Getz, D. Pu, and A. Wyglinski, Software-Defined Radio for Engineers. Norwood, MA, USA: Artech House, 2018.



Vincenzo Carotenuto (Senior Member, IEEE) received the Dr. Eng. degree in telecommunication engineering and the Ph.D. degree in electronic and telecommunication engineering from the University of Naples Federico II, Naples, Italy, in 2010 and 2015, respectively.

From September to December 2022, he was a Visiting Researcher with the Delft University of Technology, Delft, The Netherlands. He is currently an Assistant Professor with the University of Naples Federico II. His research interests in-

clude statistical signal processing, with a focus on radar signal processing.

Dr. Carotenuto was the corecipient of the Best Radar Paper Award at the 2018 and 2023 IEEE International Workshop on Metrology for Aerospace for his contributions titled "Assessing Spectral Compatibility Between Radar and Communication Systems on Measured Data" and "Experimental Evaluation of Radar Waveforms for Spectral Coexistence using the PARSAX radar," respectively.



Antonio De Maio (Fellow, IEEE) received the Dr. Eng. (Hons.) and Ph.D. degrees in information engineering from the University of Naples Federico II, Naples, Italy, in 1998 and 2002, respectively.

From October to December 2004, he was a Visiting Researcher with the U.S. Air Force Research Laboratory, Rome, NY, USA. From November to December 2007, he was a Visiting Researcher with the Chinese University of Hong Kong, Hong Kong. He is currently a

Professor with the University of Naples Federico II. His research interest includes statistical signal processing, with emphasis on radar detection, optimization theory applied to radar signal processing, and multiple-access communications.

Dr. Miao was the recipient of the 2010 IEEE Fred Nathanson Memorial Award as the young (less than 40 years of age) AESS Radar Engineer 2010 whose performance is particularly noteworthy as evidenced by contributions to the radar art over a period of several years, which the following citation for "Robust CFAR detection, knowledge-based radar signal processing, and waveform design and diversity." He was the corecipient of the 2013 best paper award (entitled to B. Carlton) of the IEEE Transactions on Aerospace and Electronic Systems with the contribution "Knowledge-Aided (Potentially Cognitive) Transmit Signal and Receive Filter Design in Signal-Dependent Clutter." He was also the recipient of the 2024 IEEE Warren White Award for outstanding achievements due to a major technical advance (or series of advances) in the art of radar engineering, with the citation "For Contributions to Radar Signal Processing Techniques for Target Detection, Waveform Design, and Electronic Protection."



Augusto Aubry (Senior Member, IEEE) received the Dr. Eng. degree in telecommunication engineering (with honors) and the Ph.D. degree in electronic and telecommunication engineering from the University of Naples Federico II, Naples, Italy, in 2007 and 2011, respectively.

From February to April 2012, he was a Visiting Researcher with Hong Kong Baptist University, Hong Kong. He is currently an Associate Professor with the University of Naples Federico II. His research interests include statistical signal

processing and optimization theory, with emphasis on MIMO communications and radar signal processing.

Dr. Aubry was the corecipient of the 2013 Best Paper Award (entitled to B. Carlton) of the IEEE TRANSACTIONS ON AEROSPACE AND ELECTRONIC SYSTEMS with the contribution "Knowledge-Aided (Potentially Cognitive) Transmit Signal and Receive Filter Design in Signal-Dependent Clutter." He was the recipient of the 2022 IEEE Fred Nathanson Memorial Award as the young (less than 40 years of age) AESS Radar Engineer 2022, with the following citation "For outstanding contributions to the application of modern optimization theory to radar waveform design and adaptive signal processing."



Francesco Fioranelli (Senior Member, IEEE) received the Laurea (B.Eng., cum laude) and Laurea Specialistica (M.Eng., cum laude) degrees in telecommunication engineering from Università Politecnica delle Marche, Ancona, Italy, in 2007 and 2010, respectively, and the Ph.D. degree in electronic engineering from Durham University, Durham, U.K., in 2014.

He was an Assistant Professor with the University of Glasgow, Glasgow, U.K., from 2016 to 2019, and a Research Associate with University

College London, London, U.K., from 2014 to 2016. He is currently an Associate Professor with the Delft University of Technology, Delft, The Netherlands. He has authored over 140 publications between book chapters, journal articles, and conference papers, and edited the book *Micro-Doppler Radar and Its Applications* (IET-Scitech, 2020). His research interests include the development of radar systems and automatic classification for human signatures analysis in healthcare and security, drones and unmanned aerial vehicle detection and classification, automotive radar, wind farm, and sea clutter.

Dr. Fioranelli was the recipient pf three best paper awards.



Oleg A. Krasnov received the M.Sc. degree in radio physics from Voronezh State University, Voronezh, Russia, in 1982, and the Ph.D. degree in radio technique from the National Aerospace University "Kharkov Aviation Institute," Kharkiv, Ukraine, in 1994.

In 1999, he joined the International Research Center for Telecommunications and Radar, Delft University of Technology (TU Delft), Delft, The Netherlands. Since 2009, he has been a Senior Researcher with the Microwave Sensing, Sig-

nals, and Systems section of the Faculty of Electrical Engineering, Mathematics, and Computer Science, TU Delft, where he became an Universitair Docent (Assistant Professor), in 2012. His research interests include radar waveforms, signal and data processing algorithms for polarimetric radars and distributed radar systems, multisensor atmospheric remote sensing, and optimal resource management of adaptive radar sensors and distributed systems.

Dr. Krasnov served as the Secretary of the 9th European Radar Conference, Amsterdam, The Netherlands.



Fred van der Zwan was born in The Hague, The Netherlands. He received the Diploma degree in electronics from the Electronic Technical School, The Hague, the Netherlands, in 1986.

He was with institutes like Toshiba, TNO, and TU Delft, in 1992, after which he became an Electronic Designer with the Telecommunications and Tele-Observation Technology Group. He initiated and coordinated several new radar projects and campaigns. He had many contacts with all participating partners in several projects.

In 2004, he became a Co-applicant of the PARSAX Project which was granted in December 2005. He became a Technical Coordinator of the PARSAX Project. In 2010, he became a Technical Coordinator with the Radar Department. In 2017, he became a Drone Pilot. He wrote an operational manual and received a certificate to perform drone flights for research purposes for Delft University of Technology (TU Delft), Delft, The Netherlands. He is currently with the Faculty of Electrical Engineering, Mathematics, and Computer Science, Microwave Sensing, Signals, and Systems Section, TU Delft.



Alexander Yarovoy (Fellow, IEEE) received the Diploma degree (Hons.) in radiophysics and electronics and the Candidate Phys. and Math.Sci. and Doctor Phys. and Math.Sci. degrees in radiophysics from Kharkov State University, Kharkiv, Ukraine, in 1984, 1987, and 1994, respectively.

In 1987, he joined the Department of Radiophysics, Kharkov State University, as a Researcher, where he became a Professor in 1997. From September 1994 to 1996, he was with the

Technical University of Ilmenau, Ilmenau, Germany, as a Visiting Researcher. Since 1999, he has been with the Delft University of Technology, Delft, The Netherlands. Since 2009, he has been leading the Chair of Microwave Sensing, Systems and Signals. He has authored or coauthored more than 450 scientific or technical articles, four patents, and 14 book chapters. His research interests include high-resolution radar, microwave imaging, and applied electromagnetics (in particular, UWB antennas).

Dr. Yarovoy was the recipient of the European Microwave Week Radar Award for the paper that best advances the state of the art in radar technology in 2001 (together with L.P. Ligthart and P. van Genderen) and in 2012 (together with T. Savelyev). In 2010, together with D. Caratelli, he was the recipient of the Best Paper Award from the Applied Computational Electromagnetic Society. He served as a Guest Editor for five special issues of IEEE transactions and other journals. Since 2011, he has been an Associate Editor for the *International Journal of Microwave and Wireless Technologies*. He served as the General TPC Chair of the 2020 European Microwave Week, the Chair and the TPC Chair of the Fifth European Radar Conference, and the Secretary of the First European Radar Conference. He also served as the Co-Chair and the TPC Chair of the Xth International Conference on GPR. From 2008 to 2017, he served as the Director for the European Microwave Association.

Open Access provided by 'Università degli Studi di Napoli "Federico II" within the CRUI CARE Agreement